ENVIRONMENTAL RESEARCH
CLIMATE

Regional tropical rainfall shifts under global warming: an energetic perspective

To cite this article before publication: Paul A Nicknish *et al* 2023 *Environ. Res.: Climate* in press https://doi.org/10.1088/2752-5295/acb9b0

Regional Tropical Rainfall Shifts Under Global Warming: An Energetic Perspective

Paul A. Nicknish[1], John C. H. Chiang[2,3], Aixue Hu[4], William R. Boos[1]
[1]*Department of Earth and Planetary Science, University of California, Berkeley, California, USA*
[2]*Department of Geography, University of California, Berkeley, California, USA*
[3]*Research Institute for Environmental Changes, Academia Sinica, Taipei, Taiwan*
[4]*Climate and Global Dynamics Division, National Center for Atmospheric Research, Boulder, Colorado, USA*

Abstract

Future climate simulations feature pronounced spatial shifts in the structure of tropical rainfall. We apply a novel atmospheric energy flux analysis to diagnose late 21st century tropical rainfall shifts in a large ensemble of simulations of 21st century climate. The method reconstructs 2D spatial changes in rainfall based on horizontal shifts in the lines of zero meridional and zonal divergent energy flux, called the energy flux equator (EFE) and energy flux prime meridian (EFPM), respectively. Two mai sources of future atmospheric energy flux changes, and hence rainfall shifts, are identified by the analysis: the high-latitude North Atlantic due to a weakened Atlantic Meridional Overturning Circulation that shifts tropical rainfall southwards over the greater Tropical Atlantic sector and eastern Pacific; and the eastern tropical Pacific due to a permanent El-Niño-like response that produces zonal shifts over the Maritime Continent and South America. To first order, the shifts in the EFE and EFPM mirror gross distributional changes in tropical precipitation, with a southward shift in rainfall over the tropical Atlantic, West Africa, and eastern tropical Pacific and an eastward shift over the Maritime Continent and western Pacific. When used to reconstruct future rainfall shifts in the tropical Atlantic and Sahel, the method reasonably represents the simulated meridional structure of rainfall shifts but does not do so for the zonal structures.

Keywords: Tropical Precipitation, Precipitation Shifts, Energy Flux Potential, Climate Change

1. Introduction

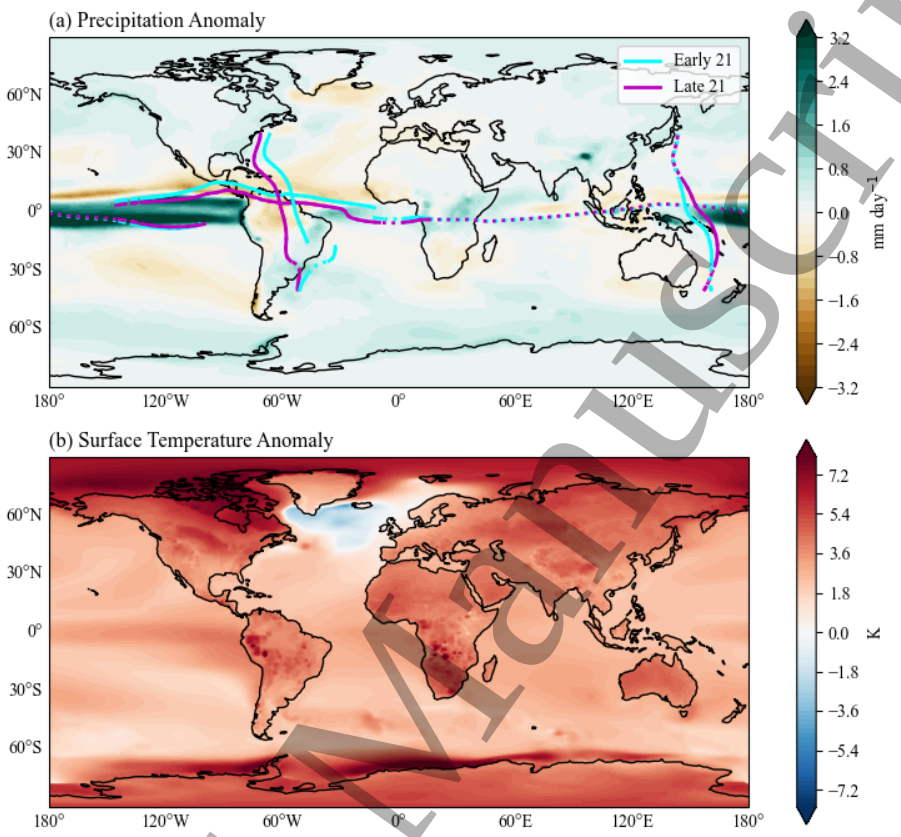

Figure 1. Late 21st century annual mean precipitation and temperature anomalies. Panel (a) shows the difference between annual mean precipitation in the late and early 21st century. Panel (b) is the same as in (a) but with surface temperature. The curves in (a) show the late (magenta) and early (cyan) 21st century EFEs and EFPMs; a solid line indicates that the shift in the EFE or EFPM is significant at the 99% confidence level.

Future projections of climate under global warming feature notable changes in the spatial patterns of tropical rainfall. Figure 1(a), for example, shows the changes in annual mean rainfall between the late (2080-2100) and early (2000-2020) 21st century from the Community Earth System Model version 2 Large Ensemble (CESM2-LE) project (Rodgers et al. 2021). In the tropics, these changes have a dipole-like structure with increases (in green) adjacent to decreases (in brown), indicative of spatial shifts (although changes in amplitude are also large). These shifts have distinct regional signatures: a southward intertropical convergence zone (ITCZ) shift over the Atlantic and eastern Pacific and an eastward shift over the Maritime Continent and western Pacific. Even slight shifts in rainfall can mean the difference between severe drought and ample rainfall for a given region (an example being the effect of Atlantic ITCZ shifts on Northeast Brazil drought, see Chiang et al. 2002). Rainfall shifts also affect atmospheric waves that cause weather: for example, longitudinal shifts in Maritime continent rainfall changes the eastward propagation characteristics of the Madden-Julian Oscillation (Wei and Ren 2019). As such, understanding the mechanisms driving these shifts is of societal importance.

Traditional interpretations of tropical rainfall changes reference local patterns in the sea surface temperature (SST) anomaly (Huang et al. 2013, Cvijanovic and Chiang 2012, Biasutti and Gianni 2006, Seager et al. 2019). The "warm gets wetter" framework (Xie et al. 2010) argues that increased precipitation corresponds to increased maxima of SST warming, and vice versa, given that surface humidity is highly correlated to local changes in SST. This interpretation would thus point to the warmer SST anomalies in the eastern equatorial Pacific and equatorial Atlantic relative to the northern subtropics (figure 1(b)) as the cause of the southward shift of the ITCZ in those regions. More generally, the "wet gets wetter" framework (Held and Soden 2006) suggests an increase in precipitation over currently wet regions and a decrease in precipitation over currently dry regions under global warming, because the pattern of precipitation minus evaporation increases proportionally with tropospheric water vapor. While these frameworks may adequately explain changes in precipitation in the zonal mean or on large spatial scales (Held and Soden 2006, Xie et al. 2010), they fall short of accurately capturing and explaining changes on regional scales and over land (see, for example, Byrne and O'Gorman 2015).

While both of these frameworks attribute rainfall changes to local properties or causes, the ultimate cause of rainfall shifts may have remote origins: for example, the southward Atlantic ITCZ shift in figure 1(a) could be the result also of the relative lack of warming over the northern subtropical Atlantic (figure 1(b)) that is linked to the absolute cooling of SST in the high latitude North Atlantic, presumably from a weakening of the Atlantic Meridional Overturning Circulation (AMOC). Similarly, zonal shifts in Indian Ocean rainfall could ultimately be a result of the pronounced warming of the eastern equatorial Pacific, in keeping with how the interannual El Niño affects Indian Ocean SST and rainfall (Shinoda et al. 2014, Yang et al. 2007). While the local SST changes associated with these rainfall shifts ultimately would have been caused by the remote influence, this fact is not immediately apparent without additional analyses. A method that is able to more directly connect rainfall shifts to these remote causes through physical principles would thus provide an interpretive advance.

A recent gain in our understanding of tropical rainfall shifts comes from studies that attribute meridional ITCZ shifts to remote high-latitude thermal forcing (Chiang and Bitz 2005, Broccoli et al. 2006). The basic mechanism behind the link between high-latitude thermal forcing and ITCZ shifts is as follows: in the presence of an excess energy input in one hemisphere, the atmosphere compensates via an increase in cross-equatorial heat transport towards the cooler hemisphere. This change in energy transport is done through a shift in the Hadley Cell, and therefore a shift in the ITCZ which lies at the ascending branch of the Hadley Cell. Kang et al. (2008, 2009) developed an energy flux framework which allows for a direct, quantitative connection between remote forcing and rainfall shifts and is based on the relationship between meridional ITCZ shifts and changes in the cross-equatorial atmospheric energy transport. Until recently however, atmospheric energy flux approaches to diagnosing rainfall shifts were limited to the zonal mean. This has been a key drawback of this method given the highly variable patterns in precipitation across longitudes. In particular, it has been shown that the zonal-mean ITCZ is an average of distinct regional ITCZs that may behave somewhat independently due to regional climate forcing (Mamalakis et al. 2021). For example, Mamalakis et. al (2021) argued that by 2100 there will be a northward shift in the ITCZ over eastern Africa and the Indian Ocean and a southward shift in the eastern Pacific and Atlantic Oceans.

In order to better understand the mechanisms of future tropical rainfall shifts and their association with remote forcings, we utilize a recently developed framework first presented in Boos and Korty (2016; hereafter BK) that generalizes the atmospheric energy flux approach to two dimensions (see also Adam et al. 2016). One of the main benefits of this method is the ability to associate changes in the atmospheric energy transport with rainfall shifts, which then allows us to attribute the rainfall changes to remote regional energy sources. Additionally, the linearity in the BK method allows us to decompose the influence of anomalous atmospheric energy transports into regional contributions, and contributions of individual flux components (latent, sensible, and radiative). Moreover, the 2-dimensional nature of the energetic perspective motivates examination of the next-century change in the 2-dimensional distribution of atmospheric energy fluxes. To this end, we identify two main centers of action in climate change scenarios: the North Atlantic (AMOC) and the eastern equatorial Pacific (permanent El Niño). We apply

this method to diagnose annual mean future tropical rainfall shifts in the CESM2-LE. Since precipitation changes in the tropical Pacific feature both amplitude changes as well as spatial shifts, we focus on and apply the theory to the greater tropical Atlantic sector, where simple spatial shifts in rainfall dominate and thus the theory is more relevant. As this is the first application of the BK method that we know of to future rainfall, we also discuss its strengths and weaknesses.

We begin by describing the data and theory used in this analysis (section 2). We then discuss contributions to and mechanisms driving future changes in atmospheric energy fluxes (section 3). We use the energy flux method to assess and reconstruct future tropical rainfall in the greater tropical Atlantic (section 4) and then finish with a summary and discussion (section 5).

2. Data and Methods

2.1 Data

We analyze model monthly mean output from the CESM2-LE (Rodgers et al. 2021), using a 10-member ensemble that was available at the time when our analysis was done. The model runs from 1850-2100 with historical forcing and the SSP370 future scenario. Initial conditions for the ensemble members are chosen from a set of 10 different years in the model's pre-industrial control run. As we are interested in changes between the late 21st century and early 21st century, we calculated the long-term annual mean over two 21-year periods, 2000-2020 and 2080-2100 (hereafter referred to as Early21 and Late21, respectively). The solver from the windspharm Python package (Dawson 2016) is used to solve the Poisson equation (equation 4, see section 2.2) on a spherical surface. We used the package's gradient function to calculate the irrotational component of the vertically integrated atmospheric energy transport, which is the component that balances the net energy input through the top and bottom of the atmosphere.

As part of the analysis, we calculated the precipitation centroids in several geographic regions to assess shifts in tropical precipitation. The longitude coordinate of the centroid is defined as

$$\text{Centroid}_{\text{lon}} = \frac{\sum_{x=a}^{b} P_{\text{mer}}\, x}{\sum_{x=a}^{b} P_{\text{mer}}} \qquad (1)$$

where P_{mer} is the meridional mean of precipitation weighted by the cosine of latitude, and a and b are the lower and upper longitudinal bounds of the region in which the centroid is calculated. The meridional mean is calculated over the latitudes of the region of interest (i.e. from c to d as defined in equation (2)). Similarly, we can define the latitude coordinate of the centroid as

$$\text{Centroid}_{\text{lat}} = \frac{\sum_{y=c}^{d} P_{\text{zon}}\, y \cos(y)}{\sum_{y=c}^{d} P_{\text{zon}} \cos(y)} \qquad (2)$$

where P_{zon} is the zonal mean of precipitation (with longitude ranging from a to b), and c and d are the lower and upper latitudinal bounds of the region of interest.

To determine the statistical significance of the shifts in the precipitation centroids between Late21 and Early21, we first computed each of these quantities for each individual ensemble member. We then calculated the difference in the latitude and longitude coordinates between Late21 and Early21 and used a two-sided Student's t-test to assess whether the differences were significantly different from 0. A 99% confidence level was used for all t-tests.

We also looked at ENSO anomalies in the CESM2 1200-year pre-industrial control run (Danabasoglu et al. 2019) (see section 3.2). Using DJF SST temperature anomalies in the cold tongue

region of the east Pacific (Deser and Wallace 1990), we determined warm and cold years. A year was considered a warm (cold) year if the DJF SST anomaly was greater (less) than 0.5 degrees. We found annual means for each of the warm and cold years and then computed the long-term mean over all the warm years and all the cold years. The "ENSO anomaly" refers to the difference between the long-term warm year mean and long-term cold year mean.

2.2 Theory

We next outline the framework for analyzing regional ITCZ shifts developed in BK and later applied in Lintner and Boos (2019). The crux of the framework relates precipitation shifts to horizontal atmospheric energy transport changes. Following BK, the energy flux potential is defined to be

$$\nabla^2 \chi = \nabla \cdot \int_0^{p_s} \boldsymbol{v} h \frac{\mathrm{d}p}{g} \qquad (3)$$

where $\boldsymbol{v}$ is vector wind, $h = c_p T + L_v q + \Phi$ is moist static energy, g is gravitational acceleration, and integration is from the top of the atmosphere to the surface pressure p_s. Following the derivation from Neelin (2007) and Lintner and Boos (2019), we can approximate the energy flux potential as

$$\nabla^2 \chi \approx E + R + H \qquad (4)$$

where E is the net surface latent heat flux, R is the net radiative energy flux into the column, and H is the net surface sensible heat flux. We use the convention that positive values indicate fluxes into the atmospheric column, and the net energy input (NEI) into the column is the sum of the net latent, sensible, and radiative fluxes. This formulation (equation 4) assumes that atmospheric energy storage is negligible, a reasonable assumption for the annual mean. The gradient of χ then gives the horizontal divergent atmospheric energy transport, which is denoted as

$$(\partial_x \chi, \partial_y \chi) = (u_h, v_h) \qquad (5)$$

but with all derivative operators taken in spherical coordinates.

In a meridional overturning circulation, the rising branch of the circulation approximately coincides with an energy flux equator (EFE), that is, a latitude where horizontal energy transports are both zero and diverging meridionally i.e. $v_h = 0$ and $\partial_y v_h > 0$. Along the same lines, the ascending branch of a zonal overturning circulation coincides with an energy flux prime meridian (EFPM), a longitude at which $u_h = 0$ and $\partial_x u_h > 0$. Recalling that the zonal-mean ITCZ and thus peak tropical precipitation lie within the rising branch of the Hadley circulation, we see the ITCZ and related precipitation band correspond with the zonal-mean EFE. BK further generalizes this notion, assuming that shifts in the regional tropical precipitation distribution mirror those of the regional EFE or EFPM. That is, for two states with different EFE and EFPM locations, we can relate the precipitation fields via a simple remapping,

$$P_2(\phi - \phi', \lambda - \lambda') = P_1(\phi, \lambda) \qquad (6)$$

The latitude and longitude shifts, ϕ' and λ' are given by

$$\phi' = (\phi_{0,2} - \phi_{0,1})\Theta(\Delta\phi - |\phi - \phi_{0,1}|) \quad (7)$$

$$\lambda' = (\lambda_{0,2} - \lambda_{0,1})\Theta(\Delta\lambda - |\lambda - \lambda_{0,1}|) \quad (8)$$

where $\phi_{0,i}$ and $\lambda_{0,i}$, denote for a climate state i, the EFE and the EFPM, respectively, Θ is the Heaviside function, and $\Delta\phi$ and $\Delta\lambda$ indicate the range of influence of the EFE and EFPM shifts, taken to be 20 and 50 degrees respectively. A $\pm 20°$ range of influence for the EFE roughly covers the expanse of the tropics. Although Lintner and Boos (2019) used $\Delta\lambda = 80°$, we use a smaller value of 50° here to avoid having changes in the Atlantic influence the orographic precipitation maxima over South America (this is discussed further in section 4.2).

Recent work has suggested that there is a coefficient of proportionality that relates EFE and ITCZ position (Kang et al. 2008, Clark et al. 2018, Peterson and Boos 2020). To determine the value of this coefficient in our particular application, we performed a linear regression between the decadal means of the zonal mean EFE latitude and the zonal mean precipitation centroid latitude in the 1200 year CESM2 pre-industrial control run. Through this regression we found a coefficient of proportionality of $\kappa = 0.195$, implying that for every 1 degree shift in the EFE, the precipitation centroid shifts by 0.195 degrees. This coefficient was used for shifts related to both the EFE and EFPM throughout the rest of the analysis.

Finally, we compute the significance of EFE and EFPM differences between Late21 and Early21 in the same way as for the precipitation centroid (and with the EFPM defined using divergent energy fluxes between 40°S and 40°N).

2.3 CESM2 Hosing Run

The coupled climate model used here is the CESM2 which is the newest version of the global climate model developed at the National Center for Atmospheric Research in collaboration with scientists from universities and US Department of Energy laboratories (Danabasoglu et al. 2020). Its atmospheric component is the Community Atmosphere Model version 6 (CAM6), the ocean component is the Parallel Ocean Program version 2 (POP2), the sea ice component is the CICE version 5 (CICE5), and the land surface component is the Community Land Model version 5 (CLM5). The horizontal resolution for all components is a nominal one degree and the simulated climate agrees with observations reasonably well.

The hosing experiment is branched from the CESM2 preindustrial control run which is a simulation with all external forcings fixed at 1850AD level. A constant freshwater forcing of 0.3 Sv ($1\ \text{Sv} = 10^6 \text{m}^3\text{s}^{-1}$) is uniformly distributed in the subpolar North Atlantic north of 50°N and in the Arctic. This simulation is part of the North Atlantic Hosing Model Intercomparison Project (NAHosMIP; Jackson et al. 2022).

3. Diagnosing the origins of the energy flux potential changes

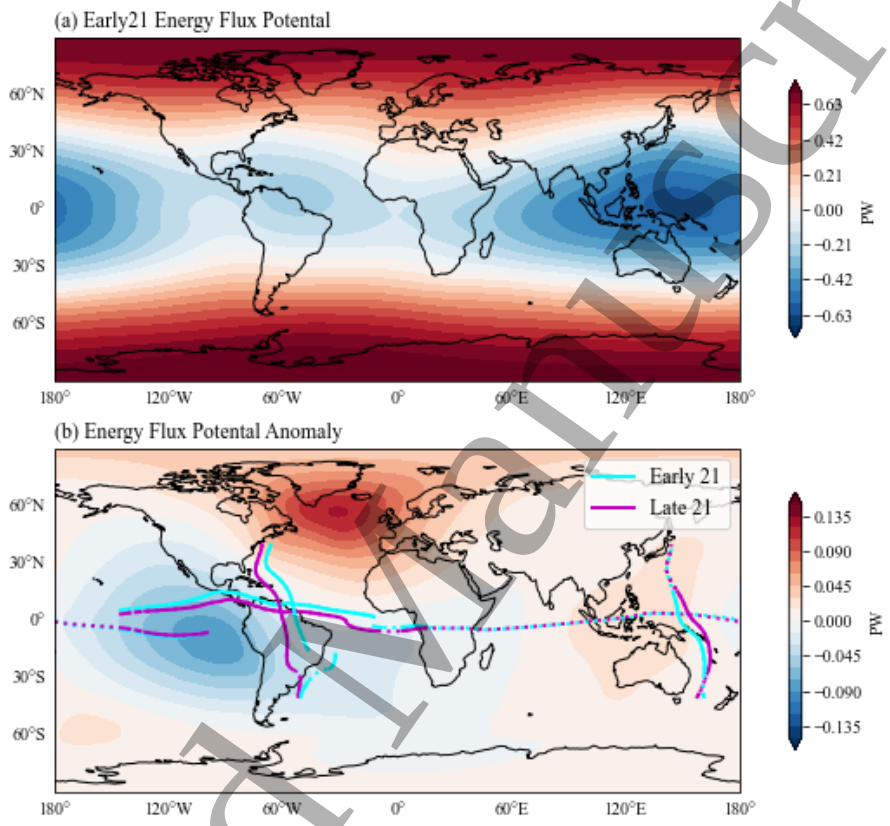

Figure 2. Energy flux potential for the early and late 21st century. (a) The annual mean energy flux potential for the early 21st century. (b) Late minus early 21st century energy flux potential. The EFE and EFPMs are shown in magenta and cyan for the late and early 21st century, respectively. The solid lines indicate where the shifts are statistically significant at the 99% confidence level.

3.1 Contributions from AMOC and the Tropical Pacific to Rainfall Shifts

Using equation (4), we calculate the ensemble- and annual-mean energy flux potential for the late and early 21st century. In general, the Early21 energy flux potential is negative throughout the tropics and positive near the poles (figure 2(a)), indicating a poleward transport of energy out of the tropics. The difference between Late21 and Early21 (figure 2(b)) reveals a strong positive center of action over the North Atlantic and a strong negative center of action over the eastern tropical Pacific. Additionally, there is a weaker positive center of action over the Maritime Continent. Note that a positive energy flux potential value generally indicates a region of increased horizontal energy flux convergence.

The difference in energy flux potential between the two time periods corresponds to a shift in the EFE and EFPMs (figure 2(b)). On a global scale, the shifts in the EFE and EFPMs (figure 2(b)) are

qualitatively consistent with the shifts in rainfall (figure 1(a)). The southward shift in the EFE over the Atlantic and Pacific accompanies the southward shift in tropical precipitation (though we note there is also a notable intensification of precipitation in the eastern Pacific as well). Additionally, there is an eastward shift in precipitation over the Maritime continent, in accord with the eastward shift in the EFPM. The EFE and EFPM shifts over these regions are statistically significant, as noted by the solid lines in figure 2b. Moreover, there is no noticeable north-south shift in the precipitation over Africa, in accord with the lack of a significant EFE shift in this region. This qualitative correspondence lends confidence to the utility of the energy flux potential method to understand future shifts in precipitation. While the traditional SST perspective would focus on local tropical Atlantic and Pacific SST changes to interpret the projected shifts in rainfall, the change in energy flux potential suggests instead that future rainfall shifts may be governed by energy fluxes into the northern Atlantic and out of the eastern equatorial Pacific.

In line with these two main centers of action in the energy flux potential anomaly, two known and notable regional changes resulting from global warming are a reduction in the AMOC and the 'ENSO-like' warming in the eastern equatorial Pacific. Previous work has shown that the AMOC is projected to weaken by nearly 50% under all SSP scenarios in simulations of the CESM2 (Hu et al. 2020). A reduced AMOC weakens the northern hemisphere monsoons and shifts the ITCZ southwards (Vellinga and Wood 2002, Zhang and Delworth 2005, Cheng et al. 2007). The warming in the eastern equatorial Pacific, on the other hand, is likely to affect tropical rainfall outside of the eastern equatorial Pacific analogous to the remote impacts of the El Niño-Southern Oscillation (ENSO) (Ropelewski and Halpert 1987, Trenberth et al. 1998). A strong El Niño event has been shown to impact remote tropical rainfall outside of the Pacific, including weakening rainfall over the Maritime Continent (Lau and Chan 1983a,b), tropical South America (Aceituno 1988) and tropical Atlantic (Saravanan and Chang 2000, Chiang et al. 2000), and strengthening rainfall over East Africa (Ropelewski and Halpert 1987, Indeje et al. 2000).

Our energy flux potential analysis for the late 21st century (figure 2(b)), with the two centers of action being the North Atlantic and eastern equatorial Pacific, suggests that the AMOC reduction and eastern equatorial Pacific warming are the two dominant regional changes that determine the EFE and EFPM shifts in the late 21st century. These two phenomena are known to involve large changes to atmospheric energy transports affecting the tropics. The reduction in northward ocean energy transport from a weakening AMOC is largely compensated for by an increase in the northward atmospheric transport over the northern hemisphere and the tropics (Cheng et al. 2007). The increased atmospheric heating over the equatorial Pacific during an El Niño event is rapidly distributed throughout the tropical belt through equatorial wave dynamics, warming the entire tropical troposphere in the process (Yulaeva and Wallace 1994, Sobel et al. 2002) and producing a shift of both EFPMs toward the East Pacific (BK).

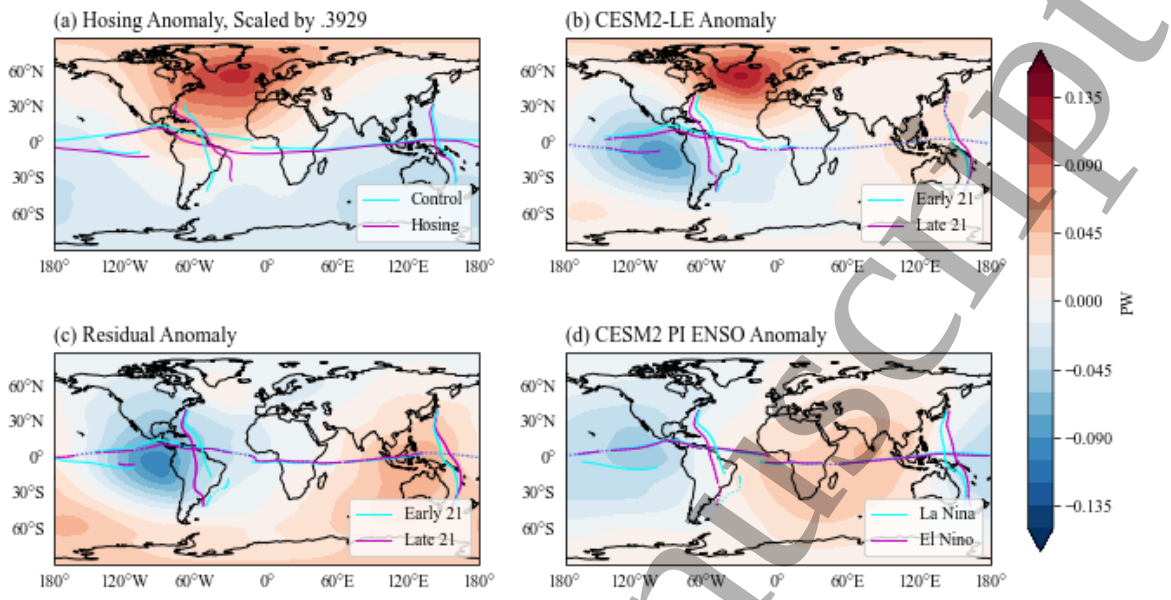

Figure 3. AMOC and ENSO-like decomposition of the energy flux potential. (a), Energy flux potential anomaly between the hosing run and the control run (see section 2.3), scaled by 0.3929. (b), Late21 minus Early21 energy flux potential in the CESM2-LE ensemble mean. Panel (c) shows the residual energy flux potential pattern after subtracting out the scaled hosing anomaly (a) from the Late21 and Early21 anomaly (b). Panel (d) shows the energy flux potential anomaly using an ENSO index in the CESM2 pre-industrial control run. While not identical, (c) and (d) both feature a more zonally asymmetric spatial pattern. This motivates labeling the residual as an "ENSO-like" pattern. In (b) and (c), the cyan curves indicate the Early21 EFE and EFPMs, and the magenta curves indicate the Late21 EFE and EFPMs. In (a) the cyan and magenta curves correspond to the control run and hosing run, respectively, and in (d) they correspond to La Nina years and El Niño years in the pre-industrial control. In panels (b), (c), and (d), solid lines indicate where the EFE and EFPM are statistically significant. Note that since there was only one hosing run, no statistical test was performed on the EFE and EFPM in panel (a).

To confirm our interpretation, we decompose the energy flux potential into an AMOC-driven component and an "ENSO-like" component. We utilize a CESM2 North Atlantic "hosing" run (see Section 2.3) in which the AMOC is significantly weakened through an influx of freshwater in the north Atlantic. The energy flux potential anomaly between the hosing run and the control run reveals a strong, positive center of action in the North Atlantic, as well as a robust meridional dipole, with negative values in the southern hemisphere and positive values in the northern hemisphere (figure 3(a)). In order to compare this anomaly to the Late21 energy flux potential anomaly (figure 3(b)), we perform a spatial regression between the energy flux potential anomaly values in the hosing simulation, with the Late21 minus Early21 energy flux potential values in the North Atlantic (50°N to 70°N, 55°W to 15°E). We find the appropriate scaling to be 0.3929 with a 95% confidence interval of (0.391, 0.395). We then subtract the scaled energy flux potential anomaly of the hosing simulation from the Late21 minus Early21 energy flux potential anomaly. This residual energy flux potential anomaly (figure 3(c)) has a zonal spatial pattern with a negative center of action in the eastern Pacific and a positive center of action over the Maritime Continent, consistent with the influence of a warm eastern equatorial Pacific SST.

For these AMOC and residual energy flux potential anomalies, we calculated the EFE and EFPM positions that result from adding these anomalies to the Early21 basic state, and compared these positions with those of the EFE and EFPM in Early21. In the AMOC contribution (figure 3(b)), there is a

substantial southward shift in the EFE in the tropical Atlantic and tropical South America, but outside of the Atlantic, there is little impact on the location of the EFE from an AMOC shutdown. In contrast, there is little EFE shift associated with the Late21 residual contribution relative to the Early21 (figure 3(c)). This shows that the southward shift in the EFE for Late21 is primarily contributed by the AMOC slowdown.

Looking at the AMOC contribution to shifts in the EFPMs, there is a slight westward shift in the Maritime Continent EFPM in the hosing run as compared to the control; over the Amazon and western Atlantic, there is a slight westward shift in the northern part of the EFPM and a more substantial eastward shift in the southern part (figure 3(a)). On the other hand, there are notable shifts in the EFPM in the Late21 residual case: an eastward shift over the Maritime Continent, and a westward shift over the Amazon Basin and west Atlantic (figure 3(c)). Thus, most of the EFPM shifts for Late21 are contributed by the influence of the warmer eastern equatorial Pacific.

This interpretation is supported by the fact that the energy flux potential and EFPM changes from El Niño events in the model's preindustrial control simulation have a similar character (figure 3(d)), though the positive center of action in the ENSO anomaly is centered over the Indian Ocean, rather than over the Maritime Continent and Australia as we see in the residual anomaly. However, the EFPM shifts are quite similar, and an exact energy flux potential pattern match is not expected as the underlying dynamics of the late 21st century warming and the interannual ENSO signal are quite different.

In conclusion, the Late21 energy flux potential change (and corresponding EFE/EFPM and precipitation shifts) in the annual mean can be thought of as having two separate contributions, one from the AMOC weakening, and the other from the El Niño-like warming in the eastern equatorial Pacific.

3.2 Regional Contributions to the EFE and EFPM

We take advantage of the linearity of the energy flux framework (equation 6) to decompose the contributions to the energy flux potential by both the flux component and the associated regional energy source. This provides insight as to which regional climate change affects tropical rainfall shifts.

We first examine the contributions of latent, sensible, and net radiative fluxes to the NEI and energy flux potential (figure 4). In the left-hand column of figure 4, we plot the contributions to the Late21 minus Early21 NEI from the latent heat flux (a), the sensible heat flux (c), and the radiative flux (e). Focusing on the North Atlantic just south of Greenland, we see a reduction in all three of the NEI components. This is consistent with an AMOC slowdown and the resulting reduced northward ocean heat transport to the North Atlantic, as reduction in the convergence of heat in this region of the ocean must be balanced by a reduction in the latent, sensible, and radiative fluxes into the atmosphere (Cheng et al. 2007, Hartmann 1994).

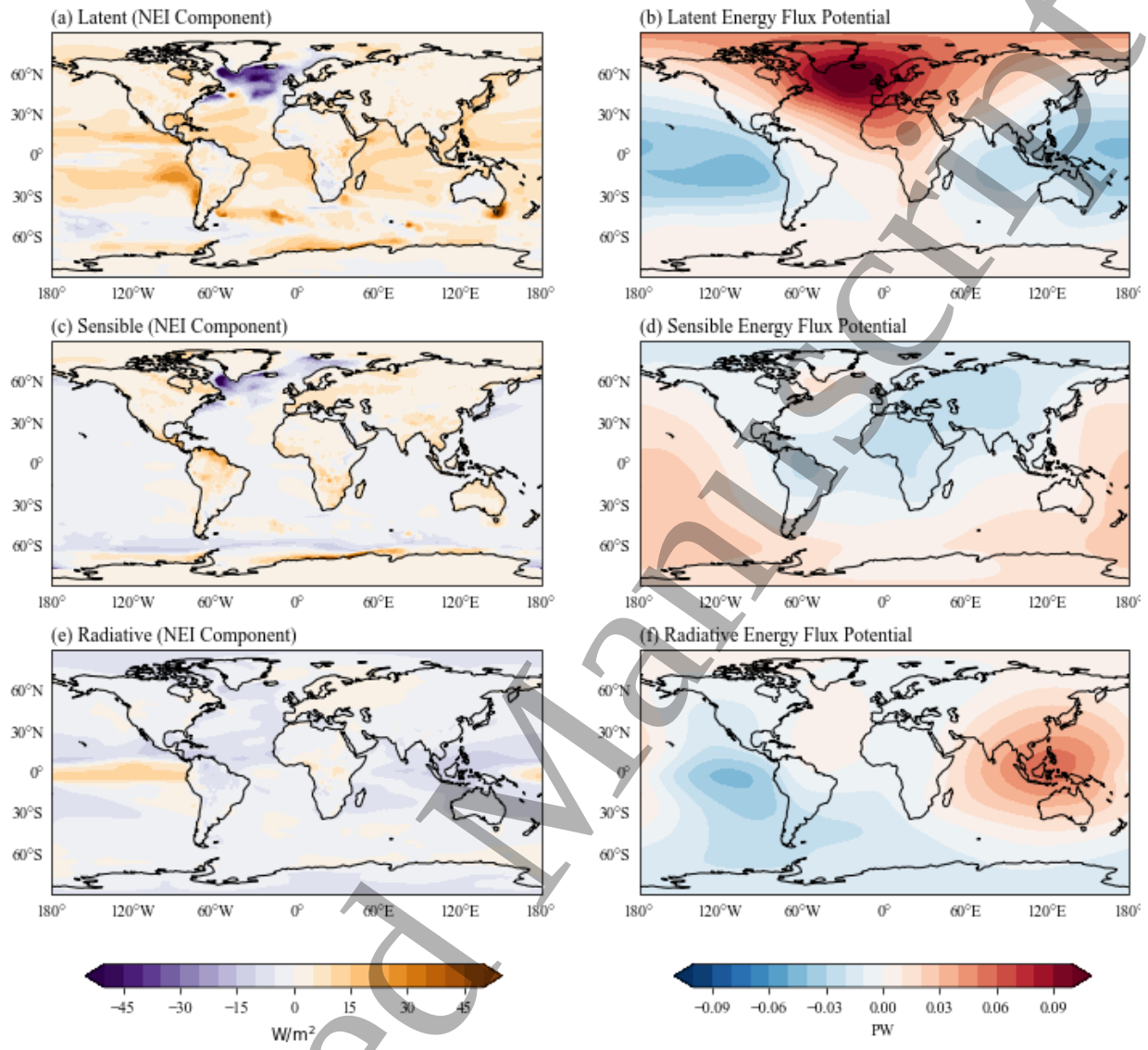

Figure 4. Latent, sensible, and radiative contributions to the Late21 anomalous NEI and energy flux potential. The lefthand column Late21 minus Early21 latent heat flux (a), sensible heat flux (c), and net radiative flux (e). The righthand column shows the breakdown of the energy flux potential anomaly between Late21 and Early21 by latent (a), sensible (b), and radiative (c) contributions. The center of action in the Northern Atlantic is largely latent driven, and the zonal pattern in the Pacific is radiative driven.

A decomposition of the energy flux potential anomaly shows that the center of action in the Northern Atlantic from figure 2(b) is largely driven by changes in latent heat flux (figure 4(b)). This suggests that changes to surface fluxes, with little radiative feedback, produce the anomaly. The contribution of the sensible heat flux (figure 4(d)) is comparatively small but has the same sign as the latent contribution in the region just south of Greenland. The contribution of radiative energy fluxes features a more zonal pattern (figure 4(f)), with a positive center of action over the maritime continent and a negative center of action over the western Pacific. A comparison between the contribution of radiative heat fluxes to the energy flux potential (figure 4(f)) and the residual energy flux potential after the AMOC influence is removed (figure 3(c), the “ENSO-like” pattern) shows that the two energy flux potential

components are similar in structure. This suggests that changes to radiative heat fluxes are largely associated with the east-west pattern in the residual; this residual is associated with zonal shifts in the Walker circulation, which alters the pattern of clouds and thus the corresponding radiative fluxes in the tropical Pacific (Peters and Bretherton 2005).

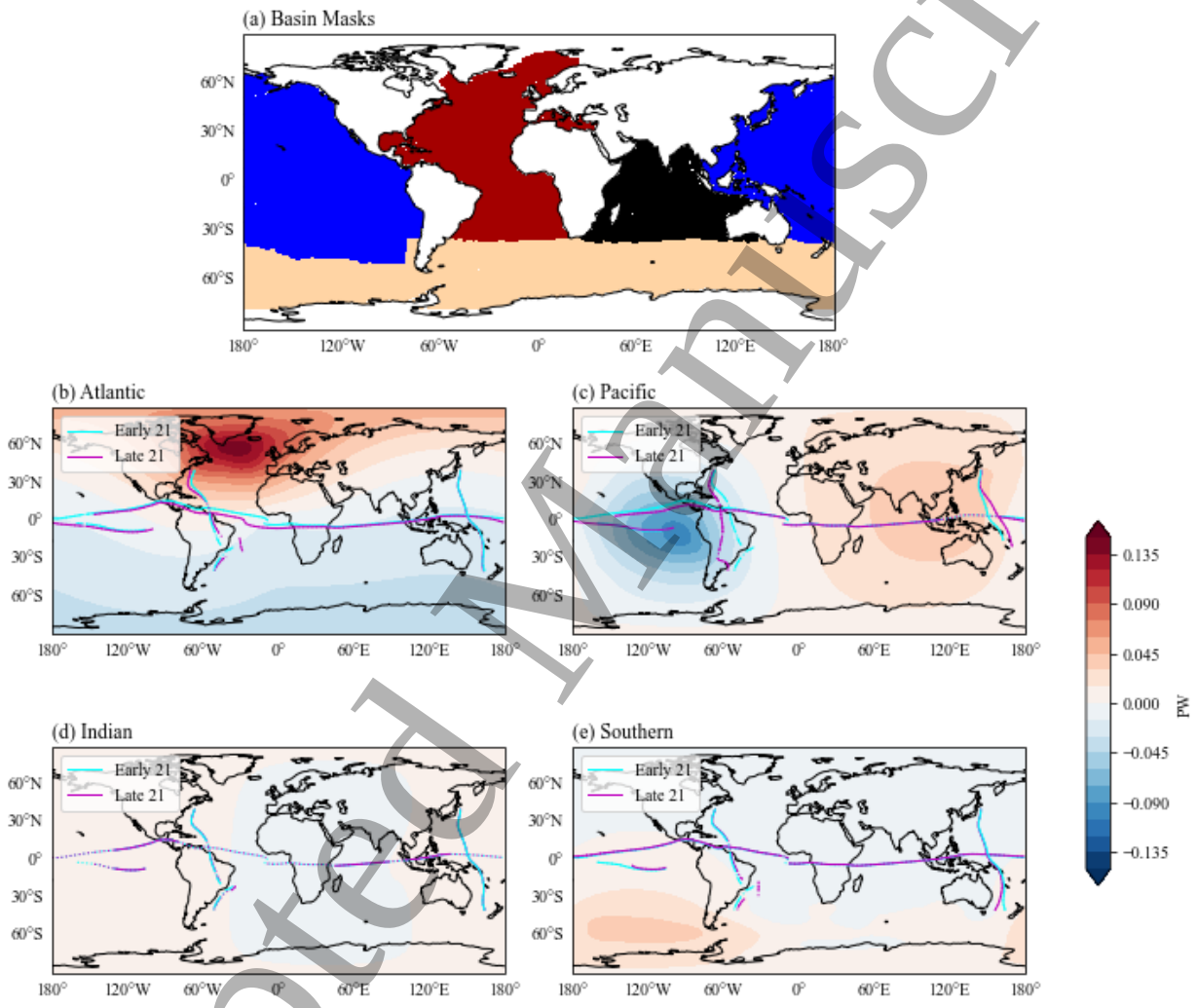

Figure 5. Ocean basin contributions to the EFE and EFPM shifts and the energy flux potential. Panel (a) shows the masks used for each of the basins with the Atlantic in red, Pacific in blue, Indian in black, and Southern in tan. Panels (b)-(e) show the energy flux potential anomaly contribution (colors) and the related EFE/EFPM shifts (cyan and magenta lines) from each of the four basins highlighted in panel (a). Panel (b) shows that for the Atlantic, (c) the Pacific, (d) the Indian, and (e) the Southern. Note that the Atlantic contribution primarily features a meridional gradient in energy flux potential and a southward shift of the EFE in the late 21st century. The Pacific on the other hand features a zonal spatial pattern and zonal shifts in the EFPMs. The other two basins have small contributions to the

energy flux potential and EFE/EFPM shifts. Solid lines indicate where shifts in the EFE or EFPM are statistically significant.

We also examine the contributions to the EFE and EFPM shift by energy sources in different ocean basins. To quantify the contribution by the Atlantic, we first select the net energy input (NEI) into the atmospheric column (sum of latent, sensible, and radiative) within that region as specified by the ocean mask shown in figure 5(a). We then create an NEI field in which values not in the Atlantic came from the Early21, and values within the Atlantic came from the Late21. The energy flux potential resulting from this regionally perturned NEI is then contrasted against the energy flux potential for Early 21.This procedure is repeated for the other ocean basins.

The results of this analysis reveal that the Atlantic, and in particular the northern Atlantic, is largely responsible for the southward shift of the EFE (figure 5(b)), associated with a strong north-south gradient in the energy flux potential anomaly. The Pacific Ocean (figure 5(c)) contributes to a strong east-west gradient in the energy flux potential, and thus dominates the zonal shift in the EFPMs but does not contribute to the southward EFE shift in the Atlantic. Of the four basins, the signal from the Indian Ocean is the weakest, contributing only a slight east-west gradient in the energy flux potential (figure 5(d)). The energy flux potential anomaly for the Southern Ocean features a modest center of action northwest of the Antarctic Peninsula, with minimal shift in the EFE (figure 5(e)). While recent work has suggested that heat uptake in the Southern Ocean reduces ocean warming over the southern hemisphere and results in a northward displacement of the tropical rain belt (Hwang et al. 2017), our results suggest that in this model the Southern Ocean influence over tropical precipitation under global warming is limited, at least for the annual mean.

In summary, the regional analysis here supports the interpretation that a weakened AMOC and the El Niño-like response are the two primary influences on annual mean atmospheric energy flux changes in future climate, which have in turn been shown to be associated with tropical rainfall shifts (Kang et al. 2008, Donohoe et al. 2013). The Pacific and Atlantic NEI anomalies contribute most to the overall energy flux potential anomaly, with the Atlantic driving most of the EFE shifts and the Pacific driving the EFPM shifts.

4. Comparison of EFE and EFPM Shifts with Rainfall

We have shown in figure 1(a) how EFE/EFPM shifts correspond, at a gross level, to tropical precipitation shifts. In this section, we evaluate more closely the ability of EFE/EFPM shifts to reconstruct, and thus explain, the simulated precipitation shifts. We first evaluate changes to the precipitation centroid, then examine changes in meridional or zonal precipitation profiles, before examining the full two-dimensional change.

4.1 Late 21st Century EFE and EFPM Shifts Over the Global Tropics

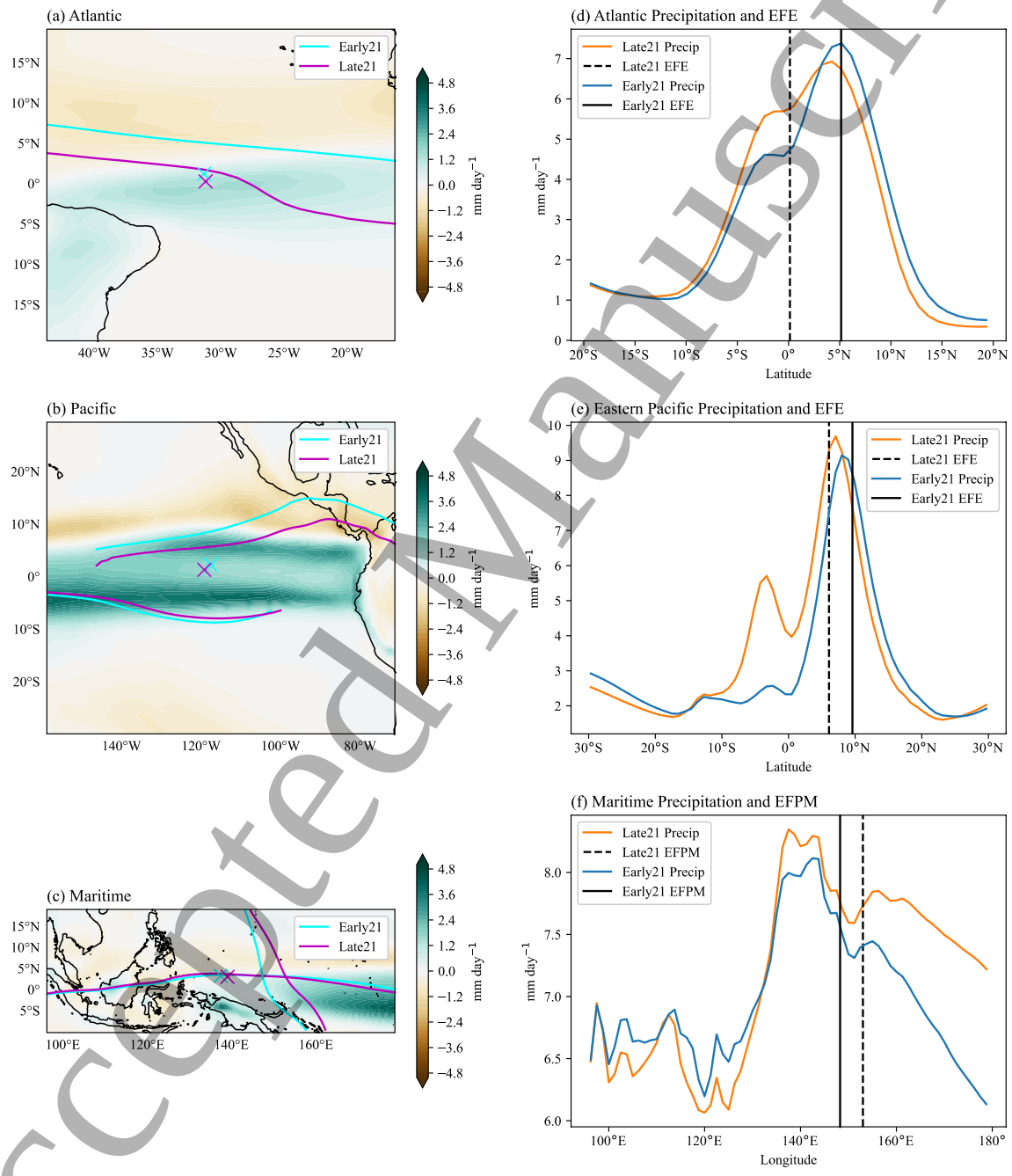

Figure 6. Comparison of EFE and EFPM shifts to changes in precipitation. Shifts in the EFE and EFPM and the corresponding changes in precipitation are shown for the (a, d) equatorial Atlantic, (b, e) equatorial eastern Pacific, and (c, f) Maritime Continent. Panels on the left show shifts in the

precipitation centroid (indicated by the 'x') and the EFE and EFPM. Contours show anomalous annual mean precipitation between Late21 and Early 21. Panels on the right show transects of zonal mean precipitation (d, e) and meridional mean precipitation (f) in the specified regions in Late21 (orange) and Early21 (blue). For panels (d) and (e), the zonal average is calculated over the longitudes shown in panels (a) and (b), respectively. For panel (f), the meridional average is calculated over the latitudes shown in panel (c). The vertical black lines in the panels on the right show the average EFE latitude (EFPM longitude in f) for Late21 (dashed) and Early21 (solid).

We first compare shifts in the EFE and EFPM to shifts in the precipitation centroid over the tropical Atlantic (20°S to 20°N, 44°W to 16°W), the eastern tropical Pacific (30°S to 30°N, 160°W to 70°W), and the Maritime continent and western Pacific (10°S to 20°N, 95°E to 180°E). In the tropical Atlantic, there is a statistically significant southward shift of the centroid, in line with the southward shift of the EFE in that region (figure 6(a)). The discrepancy in magnitude between the EFE shift and the centroid shift reflects the coefficient of proportionality between the two (see section 2.2). While there is also a slight eastward shift in the centroid in the Atlantic, we find that this is not statistically significant. In the tropical eastern Pacific, due to the double ITCZ structure in that sector, there are two divergent EFEs (and one convergent EFE, not shown, see figure 6(b); Adam et al. 2016). There is a substantial southward shift in the northern EFE, and the southern EFE shifts only slightly north. As done in Lintner and Boos (2019), when multiple EFEs are present, we can relate the shift in precipitation to the mean shift of the EFEs. Thus, the mean southward shift of the EFEs in this region is in line with the southward shift in the precipitation centroid. The tropical Pacific precipitation centroid shifts west as well, which is what we would expect given the westward shift in the EFPM in that region (figure 6(b)). Over the maritime continent and western Pacific (figure 6(c)) the shift in rainfall by the late 21st century is more zonally oriented. There is only a very slight (though statistically significant) southward shift of the precipitation centroid (the EFE shift is both very small and nonsignificant). However, in this region there is a statistically significant eastward shift of the EFPM, and correspondingly we see an eastward shift in the precipitation centroid.

We next examine changes to the zonal and meridional mean precipitation profiles and compare these to shifts in the EFE and EFPM. In the tropical Atlantic (figure 6(d)), while there are some structural changes in the precipitation pattern in Late21, notably a substantial increase in precipitation south of the equator, the Late21 zonal mean precipitation peak is generally displaced southwards relative to Early21. Also shown on the figure are the average latitudes of the Late21 and Early21 EFE (black dashed and black solid lines, respectively), highlighting the southward shift of the EFE by the late 21st century. We see that, while the EFE change suggests a much larger precipitation displacement, both the zonal mean precipitation peak and EFE in the tropical Atlantic shift south.

The tropical eastern Pacific rainfall peak around 8°N (figure 6(e)) also exhibits a clear southward shift in Late 21, as in the Atlantic. However, the most prominent feature of the Late21 rainfall is the emergence of a precipitation maximum in the southern hemisphere, indicative of the emergence of a 'double ITCZ'. Adam (2021) notes that in instances where there is strong equatorial cooling (as is the case for the equatorial eastern Pacific) and a double ITCZ situation, hemispherically asymmetric heating mainly leads to an increase in the magnitude of ITCZ rainfall in the relative warming hemisphere, rather than a spatial shift in the ITCZ peaks. This appears to be the case here, given that the northern hemisphere is the relatively cold hemisphere in this case.

Finally, over the Maritime Continent and western Pacific there is an eastward shift in the mean EFPM longitude in Late 21 relative to Early21 (figure 6(f)). The meridional mean precipitation profiles in this case indicate a distributional change in the precipitation, with decreases in the western part of the region and increases in the eastern part of the region between Late21 (figure 6(f), blue curve) and Early21 (figure 6(f), orange curve). The peak rainfall around 135°-140°E does not appear to shift in this case, but the centroid diagnostic used to characterize ITCZ changes captures this sort of change in the center-of-mass of the precipitation field (Donohoe et al. 2013).

In summary, from both qualitative inspection and calculations of shifts in the precipitation centroids and zonal and meridional mean precipitation, EFE and EFPM shifts are generally consistent with spatial changes in precipitation in Late21 in the three regions examined here. However, the precipitation changes are expressed by a combination of behaviors: (i) a shift in the precipitation maximum, as in the Atlantic ITCZ; (ii) in the case of a double ITCZ in the eastern equatorial Pacific, a relative change in the magnitudes of the two ITCZs; and (iii) a redistribution of precipitation from one side of the peak to the other, as in the western Pacific.

Given that the most pronounced EFE/EFPM changes are over the Tropical Atlantic and West African regions (figure 2(b)), and that the BK method of reconstructing rainfall involves a spatial displacement of the mean rainfall based on the EFE/EFPM changes, in the next section we focus on contrasting the BK reconstruction of rainfall changes with the actual simulated changes in the greater tropical Atlantic sector.

4.2 EFE/EFPM shifts over the Tropical Atlantic and West Africa

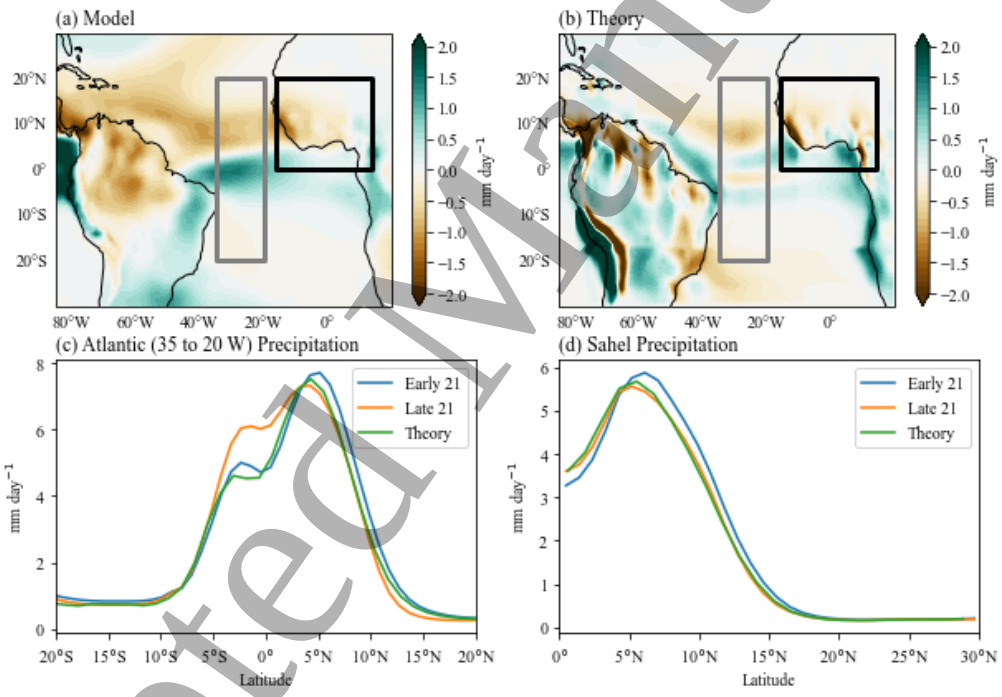

Figure 7. Theoretical reconstruction of tropical Atlantic and Sahel rainfall in the late 21st century. (a), Late 21st century anomalous precipitation from the CESM2-LE ensemble mean. (b), same as (a), but calculated using energy flux potential and the BK method. The gray box in (a) and (b) shows the region used for calculations in the tropical Atlantic and the black box indicates the Sahel. Panels (c) and (d) show the zonal mean precipitation in the tropical Atlantic and Sahel, respectively.

We applied the full 2-D method for reconstructing shifts in the precipitation distribution outlined in BK, including information from both the EFE and EFPM shifts. In comparing the anomalies using the reconstructed rainfall distribution and the model output, we focus on the tropical Atlantic and the Sahel (figure 7(a),(b)). In both the model anomaly (figure 7(a)) and the reconstructed anomaly (figure 7(b))

there is a meridional dipole structure to the rainfall anomaly between 35°W and 20°W (gray box in figure 7(a),(b)), with a decrease in rainfall to the north (from about 5°N to 10°N) and an increase in rainfall south of that (from about 10°S to 5°N). However, unlike in the model anomaly (figure 7(a)), this region of increased rainfall in the reconstructed anomaly (figure 7(b)) is interrupted by an area of decreased rainfall just south of the equator. The agreement between the two anomaly patterns breaks down over South America and just off the northeast coast of Brazil. To the east there is better agreement, with both anomalies showing a decrease in rainfall over western Africa in the Sahel (0°to 30°N, 16°W to 14°E, black box in figure 7(a),(b)). However, the reconstructed anomaly features a stronger minimum over Sierra Leone and Liberia in western Africa.

The reconstructed zonal mean precipitation profile between 35°W and 20°W in the tropical Atlantic shows good quantitative agreement with the simulated profile north of the equator, in particular with the southward shift of the precipitation peak. However, the simulated precipitation profile south of the equator shows a structural change in the rainfall pattern, indicated by the increase in zonal mean rainfall between 5°S and the equator (figure 7(c)). This feature is not captured by the reconstructed precipitation profile. Over the Sahel region, the reconstructed rainfall profile quantitatively matches the model output well (figure 7(d)). This suggests that future changes in rainfall in these regions (the tropical Atlantic north of 5°N and the Sahel) are largely the results of shifts in the existing precipitation pattern, and moreover, these shifts are captured well with this energy flux potential method, at least in a zonal mean over this region.

Over the Amazon and the South American continent there is little agreement between the theoretical rainfall anomaly and the model output, in particular along the coastlines (figure 7(a),(b)). One potential explanation is that the rainfall in that region is orographically influenced and hence pinned to the location of the topography (Chavez and Takahashi (2017)); hence, rainfall profiles cannot be readily shifted spatially. In other words, the BK framework uses no explicit information about the location of orography, so is not expected to correctly reconstruct changes in orographic precipitation maxima. For example, off the western coast of South America, we see that rainfall that was initially located over the Andes has been incorrectly shifted out over the ocean in the theoretical distribution (figure 7(b)).

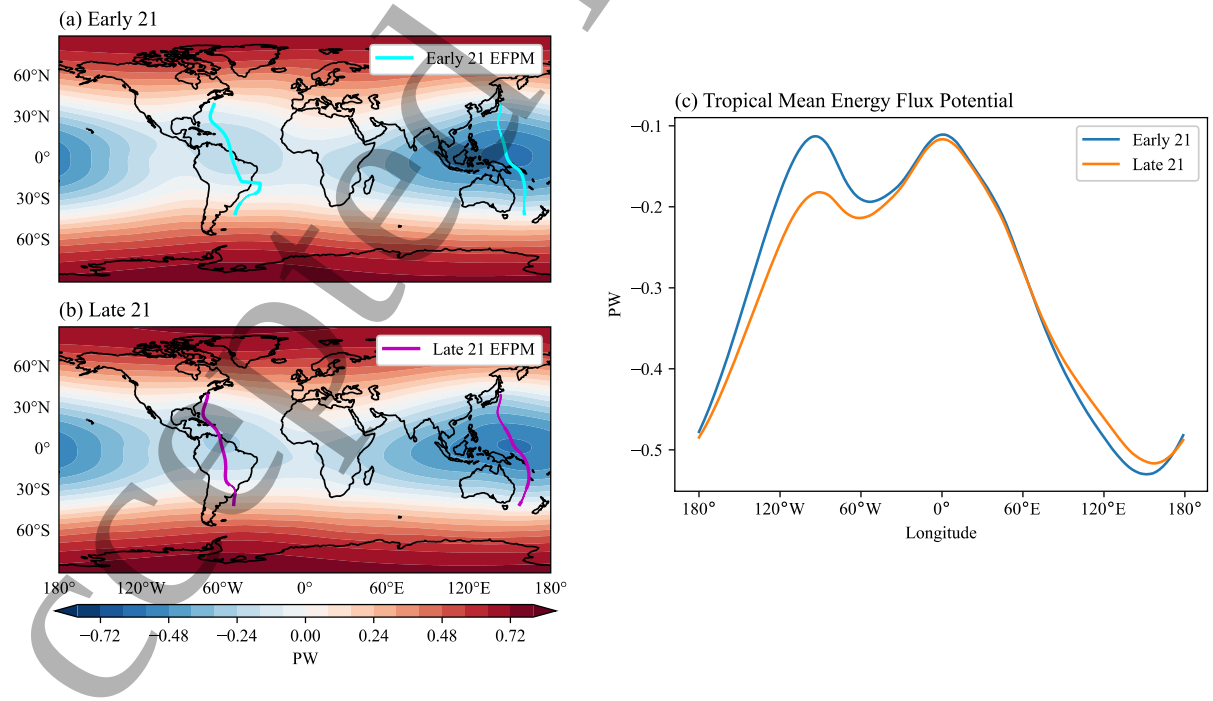

Figure 8. Tropical mean energy flux potential in the late and early 21st century. (a), Early21 and (b), Late21 energy flux potential. The Late21 EFPMs are shown in magenta and the Early21 EFPMs are shown in cyan. (c) tropical (20ºS to 20ºN) mean energy flux potential as a function of longitude.

While there is a pronounced shift in the EFPM over South America, we argue that this EFPM's influence on rainfall shifts is limited. Looking at the tropical mean energy flux potential for the Late21 and Early21 periods, we see that the EFPMs coincide with shallow local minima in the energy flux potential, as compared to the global minimum that defines the EFPM over the western Pacific (figure 8). This suggests the longitudinal range of influence of the South American EFPM is restricted. This motivates our use of 50 degrees longitude for the range of influence described in the methods sections. Additionally, we note the shifted Late21 EFPM is consistent with what happens during El Niño-events (figure 3(d)), and the influence of South American orography may prevent an energy flux method from capturing local behavior there. Nevertheless, in the course of the previous calculations, both the influence of the EFE and EFPM were included.

5. Summary and Discussion

5.1 Summary

We apply the method of Boos and Korty (2016) to the CESM2 large ensemble SSP370 simulations to evaluate the role of atmospheric energy transports in future tropical rainfall shifts. For the late 21st century, we find significant southward EFE shifts over the tropical Atlantic sector and the eastern equatorial Pacific. For the two EFPMs, there is a pronounced westward shift over South America, and an eastward shift over the western Pacific. The analysis reveals two driving regions of influence in the energy flux potential anomaly and associated EFE/EFPM and precipitation shifts, namely the high latitude north Atlantic and the eastern Pacific. Comparison with a North Atlantic 'hosing' run in which the AMOC is artificially weakened shows that the center of action in the north Atlantic in the late 21st century arises from a weakened AMOC, in accord with previous work showing a weakened AMOC over the course of the century in CESM models (Hu et al. 2020). After removing the AMOC contribution from the energy flux potential field, the residual features a zonal energy flux potential pattern resembling that associated with an El Niño. Our analysis thus suggests two main mechanisms associated with future changes in regional atmospheric energy transports and thus shifts in tropical precipitation--one driven by AMOC weakening and the other driven by the trend to permanent El Niño-like conditions. This interpretation is supported by another analysis quantifying the energy flux potential contribution by ocean basin: we find that the Atlantic and Pacific Basins dominate, with the former responsible for the energy flux potential anomaly in the high latitude north Atlantic, and the latter for the anomaly in the eastern equatorial Pacific. On the other hand, the Indian and Southern Oceans contribute little to the energy flux potential anomaly. Additionally, we use the linearity of the BK energy flux method to decompose the future changes into their contributions from latent, sensible, and radiative fluxes: we find that the latent heat flux contribution is most pronounced in the North Atlantic, and the radiative energy flux contribution largely sets the zonal pattern in energy flux potential.

In general, we find that shifts in the EFE and EFPM align with changes to the tropical precipitation, specifically with the change to the precipitation centroid. However, how the detailed precipitation change expresses itself as a result of the EFE/EPFM shift differs from region to region. Over the tropical Atlantic and Sahel region, the peak rainfall shifts southwards indicating a horizontal shift of those rainbands. Over the eastern equatorial Pacific, the rainfall change is expressed in the formation of a 'double-ITCZ' structure where rainfall increases in the southern ITCZ and decreases in the northern

ITCZ. Rainfall changes in the western Pacific and Maritime continent is expressed as a distributional change with increase over the western Pacific and decrease over the Maritime Continent, but the location of the peak rainfall remains the same.

5.2 Discussion

The energy flux method outlined in BK provides a complementary perspective on future shifts in tropical rainfall to that of the traditional SST-based interpretations. While local changes in SST do have important implications for tropical precipitation (Huang et al. 2013, Cvijanovic and Chiang 2012, Biasutti and Gianni 2006, Seager et al. 2019, Held and Soden 2006, Xie et al. 2010), it is well established that there are significant remote influences on tropical rainfall as well (Chiang and Bitz 2005, Broccoli et al. 2006, Shinoda et al. 2014, Yang et al. 2007). SST based interpretations provide important qualitative information on precipitation shifts and limited quantitative information (for example, the rough Clausius-Clapeyron scaling in the "warm-get-wetter" framework). The BK energy flux method, on the other hand, allows for a more quantitative understanding of precipitation shifts, through the calculation of the changing positions of the EFE and EFPM. The projected precipitation using the EFE and EFPM shifts captures, to first order, model-projected precipitation shifts throughout the tropics. However, in addition to simple spatial shifts, future rainfall anomalies also contain sizable changes in the intensity and structure of precipitation, and these are not captured by the BK method. The method also highlights the role of remote regions, namely the north Atlantic and the eastern equatorial Pacific, in driving these shifts in the EFE/EFPM and thus in the rainfall distribution.

The BK energy flux method also reveals which remote regions drive future energy transport changes and thus shifts in tropical precipitation, an insight not readily derived from an SST perspective. While recent work has suggested that the Indian Ocean reduces tropical Atlantic precipitation through a strengthening of the Walker Circulation and vertical stability (Hu and Fedorov 2019), our work suggests that the Indian Ocean plays little explicit role in global energy transports and the resulting precipitation shifts, at least for the annual mean. On the other hand, while the precipitation composite anomaly (figure 1(a)) shows a redistribution of precipitation over the Indian Ocean and eastern Africa, there is no EFE or EFPM in this region to help explain these changes, thus highlighting a limitation to the BK framework; an EFPM does, however, appear over the Indian region in boreal summer. Hwang et al. 2017 have suggested that the Southern Ocean also has a remote influence on tropical precipitation. Our results show that while there is a small center of action off the coast of Antarctica around 170°W (figure 2(b)), the impact of this on the tropical EFE and EFPM positions, and thus tropical precipitation, is limited. Our study however only applies to annual mean changes, which may account for why our conclusions differ from the above studies. A natural extension of this work is to examine seasonal tropical rainfall shifts in future climate using the BK method.

Since this is the first detailed examination of the method outlined in BK to future rainfall shifts that we know of, we also highlight some of the strengths and weaknesses of the method. The method generally does a good job capturing the precipitation shifts and the energy sources driving them in the greater tropical Atlantic region. There are, however, aspects of future rainfall changes that are not accounted for in the BK method. In regions where precipitation maxima are orographically constrained, rainfall can be relatively insensitive to spatial shifts in energy fluxes. In the future rainfall anomaly calculated with the BK method (figure 7(b)), we see this prominently over the Andes in South America (where the reconstructed precipitation maximum incorrectly shifts out into the Pacific Ocean). Additionally, the BK method does not capture changes in the structure or intensity of precipitation. For example, the situation in the equatorial eastern Pacific is complicated by the presence of the double ITCZ (Adam 2021) and the fact that increased surface fluxes over the cold tongue region (from enhanced SSTs, see figure 1(b)) implies an increase in rainfall unrelated to spatial shifts. In the tropical Atlantic there is an

intensification of Late21 precipitation south of the equator that similarly is not captured with a spatial shift.

Lastly, we want to highlight that this paper only applies the BK method to one model, the CESM2-LE under the SSP370 scenario, and more work should be done using this method with other models and radiative forcing scenarios. These may feature different responses in energy fluxes and precipitation, and applying this method across the full range of models and forcing scenarios could help provide a more complete picture of future energy flux-driven tropical rainfall shifts.

Overall, the energy flux potential method enables us to assess remote influences on shifts in tropical precipitation. This provides a complementary understanding to that gained from the SST perspective, which focuses on local forcings. Furthermore, the energetic perspective allows for a more quantitative understanding of precipitation shifts, through the calculation of the changing positions of the EFE and EFPM. While the reconstructed precipitation distribution from this method has limitations, it nonetheless provides a useful first-order quantitative assessment of future global energy fluxes and their impact on precipitation shifts.

7. References

Aceituno, P., 1988. On the Functioning of the Southern Oscillation in the South American Sector. Part I: Surface Climate. Mon. Wea. Rev. 116, 505–524. https://doi.org/10.1175/1520-0493(1988)116<0505:OTFOTS>2.0.CO;2

Adam, O., 2021. Dynamic and Energetic Constraints on the Modality and Position of the Intertropical Convergence Zone in an Aquaplanet. Journal of Climate 34, 527–543. https://doi.org/10.1175/JCLI-D-20-0128.1

Adam, O., Bischoff, T., Schneider, T., 2016. Seasonal and Interannual Variations of the Energy Flux Equator and ITCZ. Part II: Zonally Varying Shifts of the ITCZ. Journal of Climate 29, 7281–7293. https://doi.org/10.1175/JCLI-D-15-0710.1

Biasutti, M., Giannini, A., 2006. Robust Sahel drying in response to late 20th century forcings. Geophys. Res. Lett. 33, 2006GL026067. https://doi.org/10.1029/2006GL026067

Boos, W.R., Korty, R.L., 2016. Regional energy budget control of the intertropical convergence zone and application to mid-Holocene rainfall. Nature Geosci 9, 892–897. https://doi.org/10.1038/ngeo2833

Broccoli, A.J., Dahl, K.A., Stouffer, R.J., 2006. Response of the ITCZ to Northern Hemisphere cooling: ITCZ RESPONSE TO N. HEMISPHERE COOLING. Geophys. Res. Lett. 33, n/a-n/a. https://doi.org/10.1029/2005GL024546

Byrne, M.P., O'Gorman, P.A., 2015. The Response of Precipitation Minus Evapotranspiration to Climate Warming: Why the "Wet-Get-Wetter, Dry-Get-Drier" Scaling Does Not Hold over Land*. Journal of Climate 28, 8078–8092. https://doi.org/10.1175/JCLI-D-15-0369.1

Chavez, S.P., Takahashi, K., 2017. Orographic rainfall hot spots in the Andes-Amazon transition according to the TRMM precipitation radar and in situ data. J. Geophys. Res. Atmos. 122, 5870–5882. https://doi.org/10.1002/2016JD026282

Cheng, W., Bitz, C.M., Chiang, J.C.H., 2007. Adjustment of the global climate to an abrupt slowdown of the Atlantic meridional overturning circulation, in: Schmittner, A., Chiang, J.C.H., Hemming, S.R. (Eds.), Geophysical Monograph Series. American Geophysical Union, Washington, D. C., pp. 295–313. https://doi.org/10.1029/173GM19

Chiang, J.C.H., 2002. Deconstructing Atlantic Intertropical Convergence Zone variability: Influence of the local cross-equatorial sea surface temperature gradient and remote forcing from the eastern equatorial Pacific. J. Geophys. Res. 107, 4004. https://doi.org/10.1029/2000JD000307

Chiang, J.C.H., Bitz, C.M., 2005. Influence of high latitude ice cover on the marine Intertropical Convergence Zone. Climate Dynamics 25, 477–496. https://doi.org/10.1007/s00382-005-0040-5

Chiang, J.C.H., Kushnir, Y., Zebiak, S.E., 2000. Interdecadal changes in eastern Pacific ITCZ variability and its influence on the Atlantic ITCZ. Geophys. Res. Lett. 27, 3687–3690. https://doi.org/10.1029/1999GL011268

Clark, S.K., Ming, Y., Held, I.M., Phillipps, P.J., 2018. The Role of the Water Vapor Feedback in the ITCZ Response to Hemispherically Asymmetric Forcings. J. Climate 31, 3659–3678. https://doi.org/10.1175/JCLI-D-17-0723.1

Cvijanovic, I., Chiang, J.C.H., 2013. Global energy budget changes to high latitude North Atlantic cooling and the tropical ITCZ response. Clim Dyn 40, 1435–1452. https://doi.org/10.1007/s00382-012-1482-1

Danabasoglu, G., Lawrence, D., Lindsay, K., Lipscomb, W., Strand, G., 2019. NCAR CESM2 model output prepared for CMIP6 CMIP piControl. https://doi.org/10.22033/ESGF/CMIP6.7733

Dawson, A., 2016. Windspharm: A High-Level Library for Global Wind Field Computations Using Spherical Harmonics. JORS 4, 31. https://doi.org/10.5334/jors.129

Deser, C., Wallace, J.M., 1990. Large-Scale Atmospheric Circulation Features of Warm and Cold Episodes in the Tropical Pacific. J. Climate 3, 1254–1281. https://doi.org/10.1175/1520-0442(1990)003<1254:LSACFO>2.0.CO;2

Hartmann, D.L., 1994. Global physical climatology, International Geophysics. Academic Press, San Diego.

Held, I.M., Soden, B.J., 2006. Robust Responses of the Hydrological Cycle to Global Warming. Journal of Climate 19, 5686–5699. https://doi.org/10.1175/JCLI3990.1

Hu, A., Van Roekel, L., Weijer, W., Garuba, O.A., Cheng, W., Nadiga, B.T., 2020. Role of AMOC in Transient Climate Response to Greenhouse Gas Forcing in Two Coupled Models. Journal of Climate 33, 5845–5859. https://doi.org/10.1175/JCLI-D-19-1027.1

Hu, S., Fedorov, A.V., 2019. Indian Ocean warming can strengthen the Atlantic meridional overturning circulation. Nat. Clim. Chang. 9, 747–751. https://doi.org/10.1038/s41558-019-0566-x

Huang, P., Xie, S.-P., Hu, K., Huang, G., Huang, R., 2013. Patterns of the seasonal response of tropical rainfall to global warming. Nature Geosci 6, 357–361. https://doi.org/10.1038/ngeo1792

Hwang, Y.-T., Xie, S.-P., Deser, C., Kang, S.M., 2017. Connecting tropical climate change with Southern Ocean heat uptake: Tropical Climate Change and SO Heat Uptake. Geophys. Res. Lett. 44, 9449–9457. https://doi.org/10.1002/2017GL074972

Indeje, M., Semazzi, F.H.M., Ogallo, L.J., 2000. ENSO signals in East African rainfall seasons. Int. J. Climatol. 20, 19–46. https://doi.org/10.1002/(SICI)1097-0088(200001)20:1<19::AID-JOC449>3.0.CO;2-0

Jackson, L., Alastrue-De-Asenjo, E., Bellomo, K., Danabasoglu, G., Hu, A., Jungclaus, J., Meccia, V., Saenko, O., Shao, A., Swingedouw, D., 2022. AMOC thresholds in CMIP6 models: NAHosMIP (other). display. https://doi.org/10.5194/egusphere-egu22-2778

Kang, S.M., Frierson, D.M.W., Held, I.M., 2009. The Tropical Response to Extratropical Thermal Forcing in an Idealized GCM: The Importance of Radiative Feedbacks and Convective Parameterization. Journal of the Atmospheric Sciences 66, 2812–2827. https://doi.org/10.1175/2009JAS2924.1

Kang, S.M., Held, I.M., Frierson, D.M.W., Zhao, M., 2008. The Response of the ITCZ to Extratropical Thermal Forcing: Idealized Slab-Ocean Experiments with a GCM. Journal of Climate 21, 3521–3532. https://doi.org/10.1175/2007JCLI2146.1

Lau, K.-M., Chan, P.H., 1983a. Short-Term Climate Variability and Atmospheric Teleconnections from Satellite-Observed Outgoing Longwave Radiation. Part I: Simultaneous Relationships. J. Atmos. Sci. 40, 2735–2750. https://doi.org/10.1175/1520-0469(1983)040<2735:STCVAA>2.0.CO;2

Lau, K.-M., Chan, P.H., 1983b. Short-Term Climate Variability and Atmospheric Teleconnections from Satellite-Observed Outgoing Longwave Radiation. Part II: Lagged Correlations. J. Atmos. Sci. 40, 2751–2767. https://doi.org/10.1175/1520-0469(1983)040<2751:STCVAA>2.0.CO;2

Lintner, B.R., Boos, W.R., 2019. Using Atmospheric Energy Transport to Quantitatively Constrain South Pacific Convergence Zone Shifts during ENSO. Journal of Climate 32, 1839–1855. https://doi.org/10.1175/JCLI-D-18-0151.1

Mamalakis, A., Randerson, J.T., Yu, J.-Y., Pritchard, M.S., Magnusdottir, G., Smyth, P., Levine, P.A., Yu, S., Foufoula-Georgiou, E., 2021. Zonally contrasting shifts of the tropical rain belt in response to climate change. Nat. Clim. Chang. 11, 143–151. https://doi.org/10.1038/s41558-020-00963-x

Neelin, J.D., 2008. Chapter 10 Moist Dynamics of Tropical Convection Zones in Monsoons, Teleconnections, and Global Warming, in: Schneider, T., Sobel, A.H. (Eds.), The Global Circulation of the Atmosphere. Princeton University Press, pp. 267–301. https://doi.org/10.1515/9780691236919-012

Peters, M.E., Bretherton, C.S., 2005. A Simplified Model of the Walker Circulation with an Interactive Ocean Mixed Layer and Cloud-Radiative Feedbacks. Journal of Climate 18, 4216–4234. https://doi.org/10.1175/JCLI3534.1

Peterson, H.G., Boos, W.R., 2020. Feedbacks and eddy diffusivity in an energy balance model of tropical rainfall shifts. npj Clim Atmos Sci 3, 11. https://doi.org/10.1038/s41612-020-0114-4

Rodgers, K.B., Lee, S.-S., Rosenbloom, N., Timmermann, A., Danabasoglu, G., Deser, C., Edwards, J., Kim, J.-E., Simpson, I.R., Stein, K., Stuecker, M.F., Yamaguchi, R., Bódai, T., Chung, E.-S., Huang, L., Kim, W.M., Lamarque, J.-F., Lombardozzi, D.L., Wieder, W.R., Yeager, S.G., 2021. Ubiquity of human-induced changes in climate variability. Earth Syst. Dynam. 12, 1393–1411. https://doi.org/10.5194/esd-12-1393-2021

Ropelewski, C.F., Halpert, M.S., 1987. Global and Regional Scale Precipitation Patterns Associated with the El Niño/Southern Oscillation. Mon. Wea. Rev. 115, 1606–1626. https://doi.org/10.1175/1520-0493(1987)115<1606:GARSPP>2.0.CO;2

Saravanan, R., Chang, P., 2000. Interaction between Tropical Atlantic Variability and El Niño–Southern Oscillation. J. Climate 13, 2177–2194. https://doi.org/10.1175/1520-0442(2000)013<2177:IBTAVA>2.0.CO;2

Seager, R., Cane, M., Henderson, N., Lee, D.-E., Abernathey, R., Zhang, H., 2019. Strengthening tropical Pacific zonal sea surface temperature gradient consistent with rising greenhouse gases. Nat. Clim. Chang. 9, 517–522. https://doi.org/10.1038/s41558-019-0505-x

Shinoda, T., Alexander, M.A., Hendon, H.H., 2004. Remote Response of the Indian Ocean to Interannual SST Variations in the Tropical Pacific. J. Climate 17, 362–372. https://doi.org/10.1175/1520-0442(2004)017<0362:RROTIO>2.0.CO;2

Sobel, A.H., Held, I.M., Bretherton, C.S., 2002. The ENSO Signal in Tropical Tropospheric Temperature. J. Climate 15, 2702–2706. https://doi.org/10.1175/1520-0442(2002)015<2702:TESITT>2.0.CO;2

Trenberth, K.E., Branstator, G.W., Karoly, D., Kumar, A., Lau, N.-C., Ropelewski, C., 1998. Progress during TOGA in understanding and modeling global teleconnections associated with tropical sea surface temperatures. J. Geophys. Res. 103, 14291–14324. https://doi.org/10.1029/97JC01444

Vellinga, M., Wood, R.A., 2002. Global Climatic Impacts of a Collapse of the Atlantic Thermohaline Circulation. Climatic Change 54, 251–267. https://doi.org/10.1023/A:1016168827653

Wei, Y., Ren, H.-L., 2019. Modulation of ENSO on Fast and Slow MJO Modes during Boreal Winter. Journal of Climate 32, 7483–7506. https://doi.org/10.1175/JCLI-D-19-0013.1

Xie, S.-P., Deser, C., Vecchi, G.A., Ma, J., Teng, H., Wittenberg, A.T., 2010. Global Warming Pattern Formation: Sea Surface Temperature and Rainfall*. Journal of Climate 23, 966–986. https://doi.org/10.1175/2009JCLI3329.1

Yang, J., Liu, Q., Xie, S.-P., Liu, Z., Wu, L., 2007. Impact of the Indian Ocean SST basin mode on the Asian summer monsoon. Geophys. Res. Lett. 34, L02708. https://doi.org/10.1029/2006GL028571

Yulaeva, E., Wallace, J.M., 1994. The Signature of ENSO in Global Temperature and Precipitation Fields Derived from the Microwave Sounding Unit. J. Climate 7, 1719–1736. https://doi.org/10.1175/1520-0442(1994)007<1719:TSOEIG>2.0.CO;2

Zhang, R., Delworth, T.L., 2005. Simulated Tropical Response to a Substantial Weakening of the Atlantic Thermohaline Circulation. Journal of Climate 18, 1853–1860. https://doi.org/10.1175/JCLI3460.1

Acknowledgements

This material is based on work supported by the U.S. Department of Energy (DOE), Office of Science, Office of Biological and Environmental Research, Climate and Environmental Sciences Division, Regional and Global Model Analysis Program, under Award SC0019367. It used resources of the National Energy Research Scientific Computing Center (NERSC), which is a DOE Office of Science User Facility. This research is also supported by the National Oceanic and Atmospheric Administration Climate Program Office under Climate Variability and Predictability Program grant NA16OAR4310171. J.C.H.C. also acknowledges support from a Visiting Professorship at Academia Sinica, funded by the Ministry of Science and Technology, Taiwan, under grant number 110-2811-M-001-554. NCAR is sponsored by the NSF under Cooperative Agreement 1852977. We acknowledge the use of model output from the CESM2 Large Ensemble project with supercomputing resources provided by the IBS Center for Climate Physics in South Korea. Computing resources for the CESM2 hosing simulation was provided by the Climate Simulation Laboratory at NCAR's Computational and Information Systems Laboratory, sponsored by the NSF. AH was supported by the Regional and Global Model Analysis (RGMA) component of Earth and Environmental Systems Modeling in the Earth and Environmental Systems Sciences Division of the U.S. Department of Energy's Office of Biological and Environmental Research (BER) via National Science Foundation IA 1947282.

Author Contributions

P.A.N. and J.C.H.C. conceived the study. P.A.N. led the data analysis, writing of the manuscript, and design of figures. A.H. provided the CESM2 hosing simulations. J.C.H.C. and W.R.B. provided helpful insights, guidance, and suggestions throughout. All authors contributed to the writing of the manuscript.

Author Information

The authors declare no competing financial interests. Correspondence and requests for materials should be addressed to P.A.N. (pnicknish2@berkeley.edu).